Published in final edited form as:
Chirality. 2009 ; 21(0 1): E231–E241. doi:10.1002/chir.20804.

Absolute Configurations of DNA Lesions Determined by Comparisons of Experimental ECD and ORD Spectra with DFT Calculations

Shuang Ding[1], **Alexander Kolbanovskiy**[2], **Alexander Durandin**[2], **Conor Crean**[2], **Vladimir Shafirovich**[2], **Suse Broyde**[1], and **Nicholas E. Geacintov**[2,*]

[1]Biology Department, New York University, Silver Complex, 31 Washington Place, New York, NY 10003

[2]Chemistry Department, New York University, Silver Complex, 31 Washington Place, New York, NY 10003

Abstract

The usefulness of modern DFT methods is considered for establishing the absolute configurations of DNA lesions by comparisons of computed and experimentally measured optical rotatory dispersion (ORD) and electronic circular dichroism (ECD) spectra. Two rigid, structurally different DNA lesions (two spiroiminodihydantoin stereoisomers and four equine estrogen 4-hydoxyequilenin – DNA stereoisomeric adducts) have been investigated. In all cases, the signs and shapes of the computed ORD spectra reproduced the experimentally measured ORD spectra, although the magnitudes of the computed ORD values are different. The computed ECD spectra also reproduced the shapes of the experimental ECD spectra rather well, but are blue-shifted by 10 – 20 nm. The assignments of the absolute configurations of the DNA lesions studied based on computed and experimental ORD and ECD spectra are fully consistent with one another. The computational DFT method shows significant promise for determining the absolute configurations of DNA lesions. Establishing the stereochemistry of DNA lesions is highly useful for understanding their biological impact, especially when sufficient amounts of material are not available for other methods of structural characterization.

Keywords

DFT; Electronic Circular Dichroism; Optical Rotatory Dispersion; spiroiminodihydantoin; stereochemistry; 4-hydoxyequilenin; DNA adducts; equine estrogen

INTRODUCTION

The mechanisms of cellular DNA damage caused by endogenous reactive oxygen and nitrogen species secreted during the inflammatory response are of considerable interest because of the potentially genotoxic nucleobase lesions that are formed (1). If not repaired by cellular DNA repair systems before DNA replication occurs, error-prone translesion

*To whom Correspondence should be addressed (ng1@nyu.edu, Tel: 212 998 8407, Fax: 212 998 8421).

synthesis can lead to mutations in genes that code for proteins that play important roles in the development and progression of many cancers. Many chemical carcinogens present in our polluted environment are metabolized to highly reactive intermediates that also form covalent adducts with cellular DNA bases. The polycyclic aromatic hydrocarbon (PAH) class of chemical carcinogens that are formed by the combustion of fossil fuels, are present in tobacco smoke and play an important role in the etiology of lung and other forms of cancer (2). The stereochemical properties of the metabolites and the stereoisomeric DNA lesions formed play an important role in their formation (2), the conformations of the DNA lesions formed (3), and their processing by biological replication (4–9) and DNA repair systems (10–13).

While the absolute configurations of most of the PAH metabolite-DNA adducts are well established (14–16), our interests have focused more recently on chemically very different stereoisomeric DNA lesions with absolute configurations that had not yet been studied. These include the stereoisomeric spiroiminodihydantoin (Sp) lesions that are oxidation products of guanine in DNA (17, 18), and DNA lesions derived from metabolites of equine estrogens equilin and equilenin that constitute the active ingredients in the hormone replacement therapy formulation *Premarin* (Figure 1). The latter is widely prescribed to alleviate post-menopausal symptoms (19) and has been associated with some adverse side effects such as enhanced risk of heart disease and breast and uterine cancer (20–24). The absolute configurations of these DNA lesions are of critical importance for understanding the biochemical processing of these stereoisomeric DNA adducts in vitro and in vivo (25–27). Unfortunately, these DNA lesions are available only in small amounts and establishing their absolute configurations is a challenge in the absence of crystal structures (28).

A review of the literature indicates that significant progress has been made in recent years on computing the chiroptical characteristics, such as optical rotatory dispersion (ORD) and electronic circular dichroism spectra (ECD) (29–45). The reliability of these methods for determining the absolute configurations of chiral organic molecules has increased substantially (46–48). The combined use of both ORD and ECD leads to more reliable assignments of absolute configurations and provides generally good agreement between computed and experimentally measured ORD and ECD spectra, although exceptions have been noted (37, 46, 49–57).

In this article, we briefly summarize the important structural and biological characteristics of the DNA lesions that motivated this work, and present a mini-review of our combined experimental and computational results (28, 58, 59). We also recall some of the findings drawn from the rich literature describing the determinations of absolute configurations of chiral organic compounds by computational methods. The microgram quantities of DNA lesions available to us necessitated the assembly of a simple but sensitive instrument for measuring the wavelength dependence of ORD. These experimentally determined spectra were then compared to computed ORD and ECD spectra, and we discuss how mass spectrometry methods were used to establish the absolute configurations of the 4-hydroxyequilenin-2’-deoxycytosine adducts (4-OHEN-C, Figure 1). While the calculated and experimental characterization of vibrational circular dichroism (VCD) spectra has

provided yet another method for studying absolute configurations (50, 51, 60–64), this approach is beyond the scope of our studies.

STRUCTURAL AND BIOLOGICAL PROPERTIES OF EQUINE ESTROGEN AND Sp LESIONS

Stereoisomeric DNA lesions derived from the reactions of 4-OHEN with DNA

Equilin and Equilenin are structurally similar to the human estrogen estrone (Figure 1) except that they possess one- and two additional double bonds, respectively (19). In living cells, these conjugated estrogen derivatives are rapidly metabolized to the catechol 4-hydroxyequilenin (4-OHEN) that, in turn, readily auto-oxidizes to the *o*-quinone form (19, 65–67). These quinoids are cytotoxic and genotoxic, and can react with dC, dA, and dG in DNA to form unusual stable, stereoisomeric cyclic bulky adducts (27, 65, 68, 69). These adducts have been detected in animals (70) and humans exposed to equine estrogens (71), suggesting that they may play a role in mammary carcinogenesis, a potentially significant adverse side effect of hormone replacement therapy (67). The metabolite 4-OHEN forms bulky covalent DNA adducts with cytosine and adenine in DNA (27), not only with strikingly different absolute configurations (72) (Figure 1), but also with opposite orientations relative to the modified bases in double-stranded DNA. These differences have an impact on the processing of these DNA lesions by cellular enzymes, although these phenomena are still poorly understood. Suzuki et al. reported that the miscoding frequencies and specificities of 4-OHEN-2'-deoxycytosine adducts in vitro were strikingly influenced by the adduct stereochemistry and DNA polymerase used (73), while Chen reported that nucleotide excision repair of these DNA lesions was also adduct stereochemistry-dependent (74).

The stereiosmeric Spiromiminodihydantoin lesions in DNA

Among the oxidatively formed DNA lesions (18, 75), the diastereomeric spiroiminodihydantoins that are oxidation products of guanine and 8-oxo-7,8-dihydroguanine in DNA, have received significant attention in recent years (17, 76–79). QM geometry optimization studies have shown that the Sp *R* and *S* enantiomers (in the absence of the deoxyribose residue) have two rigid and nearly flat rings in a near-perpendicular nonplanar orientation with respect to one another (Figure 2) (80). Because of the unique chemical structures of the Sp enantiomers, the impact of these lesions on the properties of DNA and their biological functions are of great interest. Experimental (81) and computational studies (26) have shown that the two Sp lesions severely distort the DNA duplex in a stereoisomer-dependent manner. There is evidence that the two stereoisomeric Sp lesions are processed differently during translesion bypass in vitro, and are highly mutagenic in vitro (82, 83) and in vivo (84, 85) and cause G->C and G->T transversion mutations in *E. coli* (82, 85, 86). It has also been observed that the mutational properties of these lesions in *E. coli* are stereochemistry-dependent (85). The two Sp stereoisomeric lesions are also repaired with different efficiencies via the base excision repair pathway by the human Neil1 glycosylase (87). Recently, Sp was detected in repair-deficient *Escherichia coli* cells following exposure to chromate (88), thus, suggesting that Sp may contribute to oxidative DNA damage in vivo under conditions of oxidative stress (18).

COMPUTATIONS OF ORD AND ECD

The density functional theory (DFT) has been the most widely used approach for computing and deducing the chiroptic properties of stereoisomeric compounds based on their absolute configurations. Comparisons of these characteristics with experimentally measured ORD and ECD properties provides a useful approach for determining absolute configurations of stereoisomeric molecules (40, 42). The B3LYP hybrid functional with different 6-31G(d) basis sets are commonly used, and other approaches like coupled cluster (CC) (36, 54, 89, 90) and enhanced basis sets including diffuse p-functions of hydrogen atoms (32) are in use. Complicating factors are the effects of solvent (54, 55) on solute-solvent (57) and solute-solute interactions (91), and multiple conformations (42, 53, 92) that can be affected by the solvent environment (52, 93), or by bulky substituents (56). We consider selected examples of some of these approaches for evaluating absolute configurations in the following section.

Comparisons of computed and experimental OR

Significant success has been documented in computing specific optical rotations, $[\alpha]_D$, on the optically transparent long-wavelength side of the Cotton effect region at the Sodium D-line at 589 nm. DFT calculations of $[\alpha]_D$ for a series of 65 conformationally rigid alkanes, alkenes, ketones, and miscellaneous other chiral molecules with small specific rotations showed that the sign of the predicted $[\alpha]_D$ was incorrect for only eight cases (39). In general, difficulties arise when the $[\alpha]_D$ values are small due to overlapping contributions of opposite signs from different electronic transitions that can lead to a near-cancellation of the overall specific rotation values. It is now accepted that the calculations of $[\alpha]_\lambda$ at multiple, shorter wavelengths λ is more accurate since the magnitude of the specific rotation increases with decreasing wavelength, thus leading to more accurate identifications of absolute configurations. Following a protocol first introduced by Polavarapu (94), Giorgio et al (37) systematically used the prediction of ORD curves and their comparison with experimental data for assignment of absolute configurations. With the ORD curves calculated near to but not at the frequency of the resonance, this approach provided a reliable method for the assignment of absolute configuration of both rigid and conformationally flexible molecules (37, 53, 95–97). Thus, the assignment of absolute configurations by comparison of predicted and observed ORD curves has been satisfactory, although the exact match between experiment and theory is a function of the computational methodologies used (see, for example (90)).

When the molecule of interest is conformationally flexible, the contributions of each conformer to the Boltzmann equilibrium, each with different values of specific rotations, are difficult to evaluate accurately by computational methods. The effects of solvents of different polarities on the chiroptic characteristics of the molecules can be significant because of hydrogen bonding and van der Waals intra- or intermolecular interactions that may depend on solvent, thus adding to the complexities of the analysis of absolute configurations (42, 52, 53, 92).

Most of the reported quantum mechanical ORD studies in the literature have been confined to the non-resonant region on the longer wavelength side of the Cotton effect. The calculation of the ORD in the resonant frequency region has been described by Ruud et al.

(36). Their implementation encompassed Hartree–Fock theory, multi-configurational self-consistent field theory, and Kohn–Sham DFT (98). The theoretical ORD spectra were also calculated in the resonant region by Polavarapu (41), using linear response theory, and also using the KK transform of the theoretical ECD spectrum, at different theoretical levels, namely BHLYP/6-31G*, B3LYP/6-31G*, BLYP/6-31G*, and HF/6-31G*. Good agreement was noted between experimental and predicted spectra for C_{76}, thus allowing for an unambiguous determination of the absolute configurations. Calculations with a larger aug-cc-pVDZ basis set has been attempted, but the 1700 basis functions involved with this basis set resulted in linear dependencies and convergence problems that made it difficult to pursue these calculations (41).

Wavelength dependence of ORD

Calculations of ORD values at multiple wavelengths and comparisons of computational and experimental data for assignments of absolute configurations have been described (37, 52). The ORD curves were calculated near to but not at the frequency of the resonance, following a protocol first introduced by Polavarapu (94). The calculation of ORD curves provides a more reliable method for the assignment of absolute configuration of the rigid and conformationally flexible molecules than single-wavelength $[\alpha]_D$ values (37, 95). In addition, the B3LYP density functional and three different basis sets, namely 3-21G**, MidiX and DGDZVP were used for (+)-chlorofluoroiodomethane (96).

The accuracy of assignments of absolute configurations of molecules by ab initio calculations of the optical rotation values have been improved by adding calculations of ECD (44, 45, 52, 99, 100). Good resemblance between the signs and positions in wavelength of the computed and experimental ECD spectra have been observed, although there is often a nearly uniform shift in wavelength between these spectra, and the agreement between the computed and experimental rotational strengths are less satisfying (43). Computation of CD spectra in concert with optical rotations adds robustness to the assignment of absolute configuration as demonstrated for a variety of different chiral organic molecules, where the utilization of both optical properties reinforces chiral assignment when the results derived from the two methods converge (46, 49, 51–53, 92).

In summary, the concerted use of multiple chiroptical spectroscopic methods enhances the reliability of determination of molecular absolute configurations (48). A critical element in the computation of ORD and ECD spectra is the choice of level of the basis set (34, 62). Although there are quantitative differences between computed and experimental data, which are likely due to imperfections in the density functional, the neglect of solvent and temperature effects (54), or conformational flexibility (52), these approaches provide generally reliable assignment of absolute configuration.

INSTRUMENTATION

Apparatus

Standard CD spectrometers have adequate sensitivities that allow for the convenient recording of reliable CD spectra of chiroptic materials in the tens of micromolar range. However, a commercial polarimeter available to us for measuring specific rotations required

a large volume of solution (20 cm pathlength), and was suitable for measuring optical rotations at fixed wavelengths only (e.g., at the sodium D-line of 589 nm). The synthesis of large amounts (≫ 10 mg range) of DNA lesions needed for the measurements of optical rotations using such instruments can be prohibitively labor-intensive, and thus impractical. Furthermore, as noted above, it is desirable to measure ORD spectra on the long-wavelength side of the Cotton effect since the sensitivity of the measurement increases as the wavelength is decreased and approaches the absorption band of the lowest energy electronic transition. Since a high-sensitivity instrument was not available to us for measuring ORD spectra, we constructed our own system mainly from commercially available components (Figure 3). The only, but key component, was the homebuilt operational amplifier. This feedback device was designed to maintain the output current of the photomultiplier at a constant value by adjusting the voltage applied to the photomutiplier tube in order to compensate for the differences in the incident light intensities at different wavelengths. In this manner, the recording of the wavelength dependence of the optical rotation signals was facilitated without subsequent corrections for the wavelength dependence of the sensitivity of the photomultiplier tube or the light intensity. Additional details are summarized elsewhere (58).

Performance

Using a 4 mm wide, 10 mm optical pathlength cell, we routinely measure ORD spectra using ~ 300 μg of Sp nucleosides in a sample volume of 300 μL. The performance of this system is satisfactory above 250 – 260 nm, depending on the sample. Below these wavelengths, the light levels are too low because of the inexpensive monochromator and the quartz optics utilized. Typical ORD spectra of several well known amino acids obtained with this instrument are shown in Figure 4. These spectra, particularly the positive ORD values for the L-amino acids Ala, His, Glu and Ileu, and the negative values for Proline, all in acid solution, are in qualitative agreement with the spectra reported a long time ago, although the optical rotation values in Figure 4 are ~ 2 times smaller than reported earlier (101). However, as shown elsewhere (58), our instrument yields ORD spectra of (1*R*)-(+)- and (1*S*)-(−)-camphor that are qualitatively and quantitatively in agreement with the ORD spectra published most recently (37).

COMPARISONS OF COMPUTED AND EXPERIMENTALLY MEASURED ORD AND CD SPECTRA

TDDFT computations

A combination of experimental and computational methods was used to determine the stereochemistry of several DNA lesions. The experimental and calculated ORD and ECD spectra were utilized to determine the absolute configurations of the stereoisomeric pairs that exhibited ORD and ECD of opposite signs. The specific optical rotations were calculated using *ab initio* time-dependent DFT (TDDFT) (34, 39) and Gauge-Invariant Atomic Orbital (GIAO) (32) methods. The hybrid functional B3LYP/6-311++G (2d, 2p) basis set in Gaussian 03 was employed (102) to calculate ORD values, and the excitation energies and rotational strengths. B3LYP is a widely used, state-of-the-art hybrid functional,

while the 6-311++G(2d, 2p) basis set contains diffuse functions, which reduce basis set errors in the calculated ORD values (34).

Absolute Configurations of Equine Estrogen – derived 4-OHEN-DNA adducts Adduct stereochemistry

In the reaction of 4-OHEN with oligonucleotides in vitro, 4-OHEN-dC and dA adducts are the major products (27), although guanine adducts have also been detected in vivo (70). The 4-OHEN-dC and dA adducts have the same bicyclo[3.3.1]nonane type linkage site (Figure 1) with three chiral centers connecting the nucleobase-4-OHEN ring system. However, because of some highly strained ring conformations, only four different stereoisomeric adducts are observed for each base adduct. The four stereoisomers differ from one another by the absolute configurations of substituents about the C1', C2' and C3' atoms (Figure 1). However, only the absolute configurations at C2' and C3' determine the chiroptic properties of the 4-OHEN-C and -A adducts. The unsaturated bicyclo[3.3.1]nonane type linkage site causes the conformations of the 4-OHEN-C and 4-OHEN-A base adducts to be severely restricted. The chirality of the C3' atom determines the handedness of the 4-OHEN-C/A ring systems, and the C2' chirality governs the orientation of its OH group. The *1'S,2'S,3'R*-4-OHEN-C1 and *1'R,2'R,3'S*-4-OHEN-C2 stereoisomers are a pair with inverse *R* and *S* configurations, as are the *1'S,2'R,3'R*-4-OHEN-C3 and *1'R,2'S,3'S*-4-OHEN-C4 stereoisomers. These pairs are thus nearly mirror images of one another; the symmetry is broken only by the D ring with its C18' methyl group on the equilenin rings with *S* configuration in all stereoisomers (Figure 1). In the 4-OHEN-C1/C2 pair, the C2' OH group is oriented toward the cytosine base moiety, while in the 4-OHEN-C3/C4 pair this group points toward the equilenin moiety. The characteristics of the 4-OHEN-A1/A2 and 4-OHEN-A3/A4 pairs are identical to those of the C analogs. Here we shall focus on the 4-OHEN-C adducts since the considerations for the 4-OHEN-A adducts are entirely similar (28).

Distinguishing the four experimentally observed 4-OHEN – dC reaction products C^1, C^2, C^3, and C^4

When 4-OHEN and 2'-deoxycytidine are reacted with one another in aqueous solution, four reaction products are generated that are designated by their elution order in reversed phase HPLC separation experiments using C18 columns. After complete removal of the deoxyribose group by alkaline phosphatase, the resulting 4-OHEN-cytosine nucleobase adducts are designated by the order of elution of their precursor 4-OHEN-dC adducts as the 4-OHEN-cytosine adducts C^1, C^2, C^3, and C^4. The yields of C^1 and C^2 adducts are significantly lower than the yields of the C^3 and C^4 pair of adducts at the nucleoside (68) and oligonucleotide (27) levels. As shown elsewhere (28), this difference is attributed to the unfavorable steric orientation of the C2'-OH group in the C^1 and C^2 cases which lowers the yield of products.

Molecular modeling and molecular dynamics simulation studies show that the conformations of the 4-OHEN-dC and -dA stereoisomeric adducts in DNA duplexes are specifically governed by their unique stereochemical properties (25). Since the stereochemical characteristics of these two types of adducts are similar, we focus here on the

4-OHEN-C adducts, specifically on the 4-OHEN-C3/C4 adduct because we have associated these with the experimentally observed C^3 and C^4 major products of reaction (27, 28). We found that the computed chiroptic spectra of the dC^n nucleoside and C^n nucleobase adducts (n = 1, 2, 3, or 4) are not significantly different.

ORD of 4-OHEN-C adducts

The computed and measured ORD spectra of the major C^3 and C^4 adducts are of opposite sign and symmetric to one another, within experimental error (Figure 5, top panel). The ORD (and ECD) spectra of the minor products C^1 and C^2 have the same shape and sign as the major C^3 and C^4 adducts, respectively (28). Thus, there are only two types of ORD and ECD spectra of opposite sign that we attribute to the absolute configurations of the C1'-C2'-C3' unsaturated bicyclo[3.3.1]nonane bridge (Figure 1). Calculations of single $[\alpha]_D$ values at 589 nm are positive in sign for all four 4-OHEN-C stereoisomeric adducts, while experimentally, two of the four stereoisomeric C^1, C^2, C^3, and C^4 adducts exhibit negative values of $[\alpha]_D$. This result is an illustration of the inaccuracies of computing $[\alpha]_D$ values already noted in this article, since the ORD values are intrinsically small at 589 nm. Minor changes in the electronic distribution of the wave functions may introduce changes in sign of the computed values. Therefore, single wavelength calculations of $[\alpha]_{589}$ by the presently available computation methods are not entirely reliable even with a high level basis set, at least for the 4-OHEN-C adducts. Therefore, we calculated the wavelength-dependent $[\alpha]_\lambda$ values in a wavelength region where the absolute value of the specific rotation increases sharply with decreasing wavelength (Figure 5, top panel). The values of $[\alpha]_\lambda$ were computed with the small basis set (6-31G*) because the large system under investigation was computationally intractable using the higher level (B3LYP/6-311G++(2d,2p)) basis set. The calculated ORD curves of each pair of 4-OHEN-C3/C4 and and the experimentally measured C^3/C^4 stereoisomeric adducts were compared in the 370 – 600 nm range (Figure 5). Although the quantitative fits are not exact, the absolute signs, as well as the increasing magnitude of the specific rotation, $[\alpha]_\lambda$, as the wavelength is decreased, indicate that this approach is useful for correlating the absolute configurations of the molecules to the signs of the ORD spectra. Calculations below 370 nm are less reliable since the DFT method cannot satisfactorily reproduce the wavelength dependence of ORD spectra in wavelength regions that are close to electronic absorption bands, i.e., in wavelength regions where the ORD signal abruptly changes sign (see, for example, (37)). The conformations of the 2'-OH groups, specifically the dihedral angles H-O-C2'-C1' do not change the sign and shape of the computed ORD curve (data not shown).

Assignment of the absolute configuration of the 2’-OH group by mass spectrometry methods and impact of its configuration on 4-OHEN + dC reaction yields

The computed and experimental ORD spectra are not affected by the configuration of the 2’-OH group at the C2' carbon, and the signs and shapes of the computed ORD (and ECD) spectra are indistinguishable for the 4-OHEN-C1/C3 and –C2/C4 pairs of stereoisomeric adducts, or the experimentally measured C^1/C^3 and C^2/C^4 adduct ORD (or ECD) spectra. However, we have determined the C2’-OH configurations using a mass spectrometric method based on the earlier findings of Embrechts et al. (69) who showed that the MS/MS^n

ion fragmentation patterns of C^3/C^4 can be used to distinguish the configurations of the 2'-OH groups (28).

Assignments of Absolute configurations C^3/C^4 adducts from ORD spectra

Although the computational optical $[\alpha]_\lambda$ underestimate the experimental values, the signs and shapes of the ORD spectra shown in Figure 5 (top panel), together with the MS/MS^n fragmentation patterns, suggest that the absolute configuration of the C1'-C2'-C3' bridge is (+)-*1'S,2'R,3'R*-4-OHEN-C3 in the case of C^3 adducts, and (−)-*1'R,2'S,3'S*-4-OHEN-C4 for the C^4 adducts. Similar comparisons of the 4-OHEN-C1/C2 adducts yields the assignments (+)-*1'S,2'S,3'R*-4-OHEN-C1 (experimental C^1 adduct) and (−)-*1'R,2'R,3'S*-4-OHEN-C2 for the C^2 adduct (28).

Computed ECD spectra are consistent with assignments based on ORD spectra

The ECD spectra of the reaction products C^1 and C^3 have the same sign and shape, while adducts C^2 and C^4 also have identical ECD spectra but of opposite signs to those of C^1 and C^3. The excitation energies and rotational strengths for the four 4-OHEN-C stereoisomeric adducts were computed at the B3LYP/6-31G* level with Gaussian. The length and velocity rotational strengths were in good agreement, indicating that the basis set error is small. Like the experimental ECD spectra of the C^3 and C^4 adducts, the simulated ECD spectra of 4-OHEN-C3 and –C4 adducts exhibit two major CD bands in the 240 – 400 nm region of opposite sign (Figure 5). Analogous results are observed in the case of the 4-OHEN-C1 and –C3 adduct pairs (28). The positions of the computed and experimental maxima and minima coincide in the case of 4-OHEN-C3 and the adduct C^3, and the 4-OHEN-C4 and the C^4 adduct (Figure 5). The good agreement between the computed and experimental ECD spectra (Figure 5) permits the assignment of the absolute configurations of the C1'–C3' bridge that are completely consistent with the assignments based on the ORD spectra.

In summary, either the ORD results alone, or the ECD results alone, are adequate for identifying the absolute configurations of the C1'–C2'–C3' bridge of the C^1, C^2, C^3, and C^4 4-OHEN + dC reaction products. However, the configuration of the C2’-OH group cannot be identified by chirooptic methods, and was determined by MS/MS^n fragmentation methods.

Absolute configurations of spiroiminodihydantoin diastereomers Experimental and computed ORD spectra

The diastereomeric spiroiminodihydantoin 2’ deoxynucleosides are denoted by dSp1 and dSp2, according to their elution order in reversed phase HPLC experiments using Hypercarb column (59). The nucleobases Sp1 and Sp2 were obtained by hydrolysis of the 2’-deoxynucleosides dSp1 and dSp2, respectively, as described earlier (58). The experimentally determined ORD spectra of the two nucleobases, Sp1 and Sp2, dissolved in water, are shown in Figure 6 (solid lines, top panel). The calculations of the ORD values were carried out by TDDFT methods with Gaussian 03 (102) using the QM-optimized geometry of the Sp *R* and *S* enantiomers obtained by DFT methods at the B3LYP/6-31G(d) level (80). The computed ORD values are also shown in Figure 6 (top panel, solid circles). While there are differences in the computed and measured values of the specific rotation values of the Sp

enantiomers, the wavelength dependence of the measured and computed ORD values resemble one another. The signs of the experimentally measured and computed ORD values indicate that Sp1 has (−)-*S* absolute configuration, while Sp2 has (+)-*R* absolute configuration. Recently, Karwowski et al. (103), based on a detailed analysis of 2-D NMR data of dSp1 and dSp2 2'-deoxyribonucleosides, reached an opposite conclusion concerning the absolute configurations of the Sp1 and Sp2 nucleobases, a contradiction that will need to be clarified.

Tautomeric amino vs. imino forms of Sp enantiomers

All computations were carried out for the amino Sp tautomeric forms (Figure 2). However, Sp might partially exist in the imino form, as discussed in detail in our earlier publication (80). Experimental data on the Sp amino-imino tautomer equilibrium are not available, but QM geometry optimization calculations suggest that the amino form is lower in energy by only ~1 kcal/mol than the imino form (80). We therefore computed the ORD values for the imino tautomer of Sp as well. However, the predicted sign and magnitudes of the wavelength-dependent optical rotation values for either enantiomer are indistinguishable (58). The amino-imino tautomerism therefore does not influence the assignment of the absolute configurations, nor does it account for the differences between the computed and measured specific rotation values (Figure 6).

ECD spectra

The measured ECD spectra of the enantiomeric Sp nucleobases are depicted in Figure 6 (middle and bottom panels, smooth curves), and are symmetric, as expected. The CD spectra of the individual precursor dSp1 and dSp2 nucleosides are very similar in sign and wavelength to the Sp1 and Sp2 spectra, respectively (data not shown). The vertical scales in the ECD panels in Figure 6 are expressed in mdeg/absorbance unit at 230 nm (1.0 cm pathlength) rather than in molar units because the molar extinction coefficients of the Sp nucleobases could not be established because of the small amounts of material available. The computed ECD spectra strongly resemble the experimentally measured spectra in shape and sign (Figure 6, dashed lines). The simulated spectra exhibit three CD bands in the 180 – 340 nm range that reproduce the experimental spectra except for the 10 – 20 nm blue shift relative to the experimental ECD spectra. Similar shifts of computed vs. experimentally measured ECD spectra have been reported for other systems (92). These differences are not well understood, but may be due to errors in the density functional, and the neglect of solvent and vibrational effects.

In summary, comparisons of the experimentally measured and computed ORD and ECD spectra clearly indicates that Sp1 has (−)-*S* absolute configuration, while Sp2 has (+)-*R* absolute configuration, in agreement with the ORD results.

SUMMARY AND CONCLUSIONS

The concerted use of multiple chiroptical spectroscopic methods enhances the reliability of determination of absolute configurations (48). A critical element in the computation of ORD and ECD spectra is the choice of level of the basis set (34, 62). Although there are

quantitative differences between computed and experimental data, which are likely due to imperfections in the density functional, the neglect of solvent and temperature effects, or the conformational flexibility when relevant, these approaches provide reliable assignment of absolute configurations of the DNA lesions studied up till now. Both the ORD and ECD approaches point consistently to the same identifications of absolute configurations, as found in other applications (56, 104). We find that the ECD approach is particularly useful because highly sensitive CD spectrometers are widely available. The computed ECD spectra for all three molecular systems studied resemble the signs and shapes of the experimental ECD spectra, but are nearly uniformly blue-shifted. Finally, an additional spectroscopic method,VCD, is another useful approach for the assignment of absolute configuration in addition to ECD and ORD (47, 51, 60–64).

Acknowledgments

This research was supported by NIH Grants CA112412 (NEG), ES011589 (V.S.), and by CA75449 (S.B.). Partial support for computational infrastructure and systems management was also provided by Grant CA28038 (S.B.). Components of this work were conducted in a Shared Instrumentation Facility constructed with support from Research Facilities Improvement Grant C06 RR-16572 from the National Center for Research Resources, NIH. The content is solely the responsibility of the authors and does not necessarily represent the official views of the National Cancer Institute or the National Institutes of Health.

REFERENCES

1. Dedon PC, Tannenbaum SR. Reactive nitrogen species in the chemical biology of inflammation. Arch Biochem Biophys. 2004; 423:12–22. [PubMed: 14989259]
2. Luch A. Nature and nurture - lessons from chemical carcinogenesis. Nat Rev Cancer. 2005; 5:113–125. [PubMed: 15660110]
3. Geacintov NE, Cosman M, Hingerty BE, Amin S, Broyde S, Patel DJ. NMR solution structures of stereoisometric covalent polycyclic aromatic carcinogen-DNA adduct: principles, patterns, and diversity. Chemical research in toxicology. 1997; 10:111–146. [PubMed: 9049424]
4. Chary P, Latham GJ, Robberson DL, Kim SJ, Han S, Harris CM, Harris TM, Lloyd RS. In vivo and in vitro replication consequences of stereoisomeric benzo[a]pyrene-7,8-dihydrodiol 9,10-epoxide adducts on adenine N6 at the second position of N-ras codon 61. J Biol Chem. 1995; 270:4990–5000. [PubMed: 7890605]
5. Chary P, Lloyd RS. In vitro replication by prokaryotic and eukaryotic polymerases on DNA templates containing site-specific and stereospecific benzo[a]pyrene-7,8-dihydrodiol-9,10-epoxide adducts. Nucleic Acids Res. 1995; 23:1398–1405. [PubMed: 7753632]
6. Rechkoblit O, Zhang Y, Guo D, Wang Z, Amin S, Krzeminsky J, Louneva N, Geacintov NE. trans-Lesion synthesis past bulky benzo[a]pyrene diol epoxide N2-dG and N6-dA lesions catalyzed by DNA bypass polymerases. J Biol Chem. 2002; 277:30488–30494. [PubMed: 12063247]
7. Suzuki N, Ohashi E, Kolbanovskiy A, Geacintov NE, Grollman AP, Ohmori H, Shibutani S. Translesion synthesis by human DNA polymerase kappa on a DNA template containing a single stereoisomer of dG-(+)- or dG-(−)-anti-N(2)-BPDE (7,8-dihydroxy-anti-9,10-epoxy-7,8,9,10-tetrahydrobenzo[a]pyrene). Biochemistry. 2002; 41:6100–6106. [PubMed: 11994005]
8. Seo KY, Nagalingam A, Miri S, Yin J, Chandani S, Kolbanovskiy A, Shastry A, Loechler EL. Mirror image stereoisomers of the major benzo[a]pyrene N2-dG adduct are bypassed by different lesion-bypass DNA polymerases in E. coli. DNA Repair (Amst). 2006; 5:515–522. [PubMed: 16483853]
9. Shibutani S, Margulis LA, Geacintov NE, Grollman AP. Translesional synthesis on a DNA template containing a single stereoisomer of dG-(+)- or dG-(−)-anti-BPDE (7,8-dihydroxy-anti-9,10-epoxy-7,8,9,10-tetrahydrobenzo[a]pyrene). Biochemistry. 1993; 32:7531–7541. [PubMed: 8338850]

10. Buterin T, Hess MT, Luneva N, Geacintov NE, Amin S, Kroth H, Seidel A, Naegeli H. Unrepaired fjord region polycyclic aromatic hydrocarbon-DNA adducts in ras codon 61 mutational hot spots. Cancer Res. 2000; 60:1849–1856. [PubMed: 10766171]
11. Hess MT, Gunz D, Luneva N, Geacintov NE, Naegeli H. Base pair conformation-dependent excision of benzo[a]pyrene diol epoxide-guanine adducts by human nucleotide excision repair enzymes. Mol Cell Biol. 1997; 17:7069–7076. [PubMed: 9372938]
12. Zou Y, Liu TM, Geacintov NE, Van Houten B. Interaction of the UvrABC nuclease system with a DNA duplex containing a single stereoisomer of dG-(+)- or dG-(−)-anti-BPDE. Biochemistry. 1995; 34:13582–13593. [PubMed: 7577947]
13. Geacintov NE, Broyde S, Buterin T, Naegeli H, Wu M, Yan SX, Patel DJ. Thermodynamic and structural factors in the removal of bulky DNA adducts by the nucleotide excision repair machinery. Biopolymers. 2002; 65:202–210. [PubMed: 12228925]
14. Karle IL, Yagi H, Sayer JM, Jerina DM. Crystal and molecular structure of a benzo[a]pyrene 7,8-diol 9,10-epoxide N2-deoxyguanosine adduct: absolute configuration and conformation. Proc Natl Acad Sci U S A. 2004; 101:1433–1438. [PubMed: 14757823]
15. Weems HB, Yang SK. Chiral stationary phase high-performance liquid chromatographic resolution and absolute configuration of enantiomeric benzo[a]pyrene diol-epoxides and tetrols. Chirality. 1989; 1:276–283. [PubMed: 2642055]
16. Kroth H, Yagi H, Seidel A, Jerina DM. New and highly efficient synthesis of cis- and trans-opened Benzo[a]pyrene 7,8-diol 9,10-epoxide adducts at the exocyclic N(2)-amino group of deoxyguanosine. J Org Chem. 2000; 65:5558–5564. [PubMed: 10970294]
17. Cadet J, Douki T, Ravanat JL. Oxidatively generated damage to the guanine moiety of DNA: mechanistic aspects and formation in cells. Accounts of chemical research. 2008; 41:1075–1083. [PubMed: 18666785]
18. Neeley WL, Essigmann JM. Mechanisms of formation, genotoxicity, and mutation of guanine oxidation products. Chemical research in toxicology. 2006; 19:491–505. [PubMed: 16608160]
19. Bolton JL, Pisha E, Zhang F, Qiu S. Role of quinoids in estrogen carcinogenesis. Chem Res Toxicol. 1998; 11:1113–1127. [PubMed: 9778307]
20. Hersh AL, Stefanick ML, Stafford RS. National use of postmenopausal hormone therapy: annual trends and response to recent evidence. Jama. 2004; 291:47–53. [PubMed: 14709575]
21. Okamoto Y, Chou PH, Kim SY, Suzuki N, Laxmi YRS, Okamoto K, Liu XP, Matsuda T, Shibutani S. Oxidative DNA damage in Xpc-knockout and its wild mice treated with equine estrogen. Chemical Research in Toxicology. 2008; 21:1120–1124. [PubMed: 18447394]
22. Ravdin PM, Cronin KA, Howlader N, Berg CD, Chlebowski RT, Feuer EJ, Edwards BK, Berry DA. The decrease in breast-cancer incidence in 2003 in the United States. New England Journal of Medicine. 2007; 356:1670–1674. [PubMed: 17442911]
23. Rossouw JE, Anderson GL, Prentice RL, LaCroix AZ, Kooperberg C, Stefanick ML, Jackson RD, Beresford SA, Howard BV, Johnson KC, Kotchen JM, Ockene J. Risks and benefits of estrogen plus progestin in healthy postmenopausal women: principal results From the Women's Health Initiative randomized controlled trial. Jama. 2002; 288:321–333. [PubMed: 12117397]
24. Yager JD, Davidson NE. Mechanisms of disease: Estrogen carcinogenesis in breast cancer. New England Journal of Medicine. 2006; 354:270–282. [PubMed: 16421368]
25. Ding S, Shapiro R, Cai Y, Geacintov NE, Broyde S. Conformational Properties of Equilenin-DNA Adducts: Stereoisomer and Base Effects. Chemical research in toxicology. 2008
26. Jia L, Shafirovich V, Shapiro R, Geacintov NE, Broyde S. Structural and thermodynamic features of spiroiminodihydantoin damaged DNA duplexes. Biochemistry. 2005; 44:13342–13353. [PubMed: 16201759]
27. Kolbanovskiy A, Kuzmin V, Shastry A, Kolbanovskaya M, Chen D, Chang M, Bolton JL, Geacintov NE. Base selectivity and effects of sequence and DNA secondary structure on the formation of covalent adducts derived from the equine estrogen metabolite 4-hydroxyequilenin. Chem Res Toxicol. 2005; 18:1737–1747. [PubMed: 16300383]
28. Ding S, Wang Y, Kolbanovskiy A, Durandin A, Bolton JL, van Breemen RB, Broyde S, Geacintov NE. Determination of absolute configurations of 4-hydroxyequilenin-cytosine and -adenine adducts by optical rotatory dispersion, electronic circular dichroism, density functional theory

calculations, and mass spectrometry. Chemical research in toxicology. 2008; 21:1739–1748. [PubMed: 18680315]

29. Polavarapu PL. Ab initio molecular optical rotations and absolute configurations. Molecular Physics. 1997; 91:551–554.
30. Polavarapu PL, Chakraborty DK. Absolute stereochemistry of chiral molecules from ab initio theoretical and experimental molecular optical rotations. Journal of the American Chemical Society. 1998; 120:6160–6164.
31. Kondru RK, Wipf P, Beratan DN. Theory-assisted determination of absolute stereochemistry for complex natural products via computation of molar rotation angles. Journal of the American Chemical Society. 1998; 120:2204–2205.
32. Cheeseman JR, Frisch MJ, Devlin FJ, Stephens PJ. Hartree-Fock and density functional theory ab initio calculation of optical rotation using GIAOs: Basis set dependence. Journal of Physical Chemistry A. 2000; 104:1039–1046.
33. Stephens PJ, Devlin FJ, Cheeseman JR, Frisch MJ, Mennucci B, Tomasi J. Prediction of optical rotation using density functional theory: 6,8-dioxabicyclo[3.2.1]octanes. Tetrahedron-Asymmetry. 2000; 11:2443–2448.
34. Stephens PJ, Devlin FJ, Cheeseman JR, Frisch MJ. Calculation of optical rotation using density functional theory. Journal of Physical Chemistry A. 2001; 105:5356–5371.
35. Grimme S. Calculation of frequency dependent optical rotation using density functional response theory. Chemical Physics Letters. 2001; 339:380–388.
36. Ruud K, Helgaker T. Optical rotation studied by density-functional and coupled-cluster methods. Chemical Physics Letters. 2002; 352:533–539.
37. Giorgio E, Viglione RG, Zanasi R, Rosini C. Ab initio calculation of optical rotatory dispersion (ORD) curves: A simple and reliable approach to the assignment of the molecular absolute configuration. Journal of the American Chemical Society. 2004; 126:12968–12976. [PubMed: 15469294]
38. Stephens PJ, Devlin FJ, Cheeseman JR, Frisch MJ, Bortolini O, Besse P. Determination of absolute configuration using ab initio calculation of optical rotation. Chirality. 2003; 15(Suppl):S57–S64. [PubMed: 12884375]
39. Stephens PJ, Mccann DM, Cheeseman JR, Frisch MJ. Determination of absolute configurations of chiral molecules using ab initio time-dependent density functional theory calculations of optical rotation: How reliable are absolute configurations obtained for molecules with small rotations? Chirality. 2005; 17:S52–S64. [PubMed: 15747317]
40. Polavarapu PL. Optical Rotation: Recent advances in determining the absolute configuration. Chirality. 2002; 14:768–781. [PubMed: 12395394]
41. Polavarapu PL, He JT, Crassous J, Ruud K. Absolute configuration of C-76 from optical rotatory dispersion. Chemphyschem. 2005; 6:2535–2540. [PubMed: 16270369]
42. Specht KM, Nam J, Douglas M, Ho DM, Berova N, Kondru RK, Beratan DN, Wipf P, Pascal RA Jr, Kahne D. Determining absolute configuration in flexible molecules: A case study. J. Am. Chem. Soc. 2001; 123:8961–8966. [PubMed: 11552802]
43. Wang YK, Raabe G, Repges C, Fleischhauer J. Time-dependent density functional theory calculations on the chiroptical properties of rubroflavin: Determination of its absolute configuration by comparison of measured and calculated CD spectra. International Journal of Quantum Chemistry. 2003; 93:265–270.
44. Furche F, Ahlrichs R, Wachsmann C, Weber E, Sobanski A, Vogtle F, Grimme S. Circular dichroism of helicenes investigated by time-dependent density functional theory. Journal of the American Chemical Society. 2000; 122:1717–1724.
45. Autschbach J, Ziegler T, van Gisbergen SJA, Baerends EJ. Chiroptical properties from time-dependent density functional theory. I. Circular dichroism spectra of organic molecules. Journal of Chemical Physics. 2002; 116:6930–6940.
46. Stephens PJ, McCann DM, Devlin FJ, Cheeseman JR, Frisch MJ. Determination of the absolute configuration of [3(2)](1,4) barrelenophanedicarbonitrile using concerted time-dependent density functional theory calculations of optical rotation and electronic circular dichroism. Journal of the American Chemical Society. 2004; 126:7514–7521. [PubMed: 15198598]

47. Polavarapu PL. Renaissance in chiroptical spectroscopic methods for molecular structure determination. Chemical Record. 2007; 7:125–136. [PubMed: 17394174]
48. Polavarapu PL. Why is it important to simultaneously use more than one chiroptical spectroscopic method for determining the structures of chiral molecules? Chirality. 2008; 20:664–672. [PubMed: 17924421]
49. Stephens PJ, McCann DM, Butkus E, Stoncius S, Cheeseman JR, Frisch MJ. Determination of absolute configuration using concerted ab initio DFT calculations of electronic circular dichroism and optical rotation: Bicyclo[3.3.1]nonane diones. Journal of Organic Chemistry. 2004; 69:1948–1958. [PubMed: 15058939]
50. Stephens PJ, Pan JJ, Devlin FJ, Krohn K, Kurtan T. Determination of the absolute configurations of natural products via density functional theory calculations of vibrational circular dichroism, electronic circular dichroism, and optical rotation: the iridoids plumericin and isoplumericin. The Journal of organic chemistry. 2007; 72:3521–3536. [PubMed: 17388636]
51. Stephens PJ, Pan JJ, Devlin FJ, Urbanova M, Julinek O, Hajicek J. Determination of the absolute configurations of natural products via density functional theory calculations of vibrational circular dichroism, electronic circular dichroism, and optical rotation: the iso-schizozygane alkaloids isoschizogaline and isoschizogamine. Chirality. 2008; 20:454–470. [PubMed: 17853399]
52. Kwit M, Sharma ND, Boyd DR, Gawronski J. Absolute configuration of conformationally flexible cis-dihydrodiol metabolites by the method of confrontation of experimental and calculated electronic CD spectra and optical rotations. Chemistry-a European Journal. 2007; 13:5812–5821.
53. Giorgio E, Tanaka K, Verotta L, Nakanishi K, Berova N, Rosini C. Determination of the absolute configurations of flexible molecules: Synthesis and theoretical simulation of electronic circular dichroism/optical rotation of some pyrrolo[2,3-b]indoline alkaloids - A case study. Chirality. 2007; 19:434–445. [PubMed: 17393468]
54. Crawford TD, Stephens PJ. Comparison of time-dependent density-functional theory and coupled cluster theory for the calculation of the optical rotations of chiral molecules. Journal of Physical Chemistry A. 2008; 112:1339–1345.
55. Zhang P, Polavarapu PL. Spectroscopic investigation of the structures of dialkyl tartrates and their cyclodextrin complexes. Journal of Physical Chemistry A. 2007; 111:858–871.
56. Tartaglia S, Padula D, Scafato P, Chiummiento L, Rosini C. A chemical/computational approach to the determination of absolute configuration of flexible and transparent molecules: Aliphatic diols as a case study. Journal of Organic Chemistry. 2008; 73:4865–4873. [PubMed: 18547112]
57. Mori T, Grimme S, Inoue Y. A combined experimental and theoretical study on the conformation of multiarmed chiral aryl ethers. Journal of Organic Chemistry. 2007; 72:6998–7010. [PubMed: 17665959]
58. Durandin A, Jia L, Crean C, Kolbanovskiy A, Ding S, Shafirovich V, Broyde S, Geacintov NE. Assignment of absolute configurations of the enantiomeric spiroiminodihydantoin nucleobases by experimental and computational optical rotatory dispersion methods. Chemical Research in Toxicology. 2006; 19:908–913. [PubMed: 16841958]
59. Ding S, Jia L, Durandin A, Crean C, Kolbanovskiy A, Shafirovich V, Broyde S, Geacintov NE. Absolute configurations of spiroiminodihydantoin and allantoin stereoisomers: comparison of computed and measured electronic circular dichroism spectra. Chem Res Toxicol. 2009; 22:1189–1193. [PubMed: 19485408]
60. Stephens PJ, Pan JJ, Devlin FJ, Urbanova M, Hajicek J. Determination of the absolute configurations of natural products via density functional theory calculations of vibrational circular dichroism, electronic circular dichroism and optical rotation: the schizozygane alkaloid schizozygine. The Journal of organic chemistry. 2007; 72:2508–2524. [PubMed: 17338574]
61. Stephens PJ, Devlin FJ, Gasparrini F, Ciogli A, Spinelli D, Cosimelli B. Determination of the absolute configuration of a chiral oxadiazol-3-one calcium channel blocker, resolved using chiral chromatography, via concerted density functional theory calculations of its vibrational circular dichroism, electronic circular dichroism, and optical rotation. The Journal of organic chemistry. 2007; 72:4707–4715. [PubMed: 17516678]
62. Petrovic AG, Polavarapu PL. Chiroptical spectroscopic determination of molecular structures of chiral sulfinamides: t-butanesulrinamide. Journal of Physical Chemistry A. 2007; 111:10938–10943.

63. Petrovic AG, Polavarapu PL, Drabowicz J, Lyzwa P, Mikolajczyk M, Wieczorek W, Balinska A. Diastereomers of N-alpha-phenylethyl-t-butylsulfinamide: Absolute configurations and predominant conformations. Journal of Organic Chemistry. 2008; 73:3120–3129. [PubMed: 18341347]
64. Petrovic AG, Vick SE, Polavarapu PL. Determination of the absolute stereochemistry of chiral biphenanthiryls in solution phase using chiroptical spectroscopic methods: 2,2 '-diphenyl-[3,3 '-biphenanthrene]-4,4 '-diol. Chirality. 2008; 20:501–510. [PubMed: 17963199]
65. Shen L, Pisha E, Huang Z, Pezzuto JM, Krol E, Alam Z, van Breemen RB, Bolton JL. Bioreductive activation of catechol estrogen-ortho-quinones: aromatization of the B ring in 4-hydroxyequilenin markedly alters quinoid formation and reactivity. Carcinogenesis. 1997; 18:1093–1101. [PubMed: 9163701]
66. Zhang F, Chen Y, Pisha E, Shen L, Xiong Y, van Breemen RB, Bolton JL. The major metabolite of equilin, 4-hydroxyequilin, autoxidizes to an o-quinone which isomerizes to the potent cytotoxin 4-hydroxyequilenin-o-quinone. Chem Res Toxicol. 1999; 12:204–213. [PubMed: 10027800]
67. Bolton JL, Thatcher GR. Potential mechanisms of estrogen quinone carcinogenesis. Chemical research in toxicology. 2008; 21:93–101. [PubMed: 18052105]
68. Shen L, Qiu S, Chen Y, Zhang F, van Breemen RB, Nikolic D, Bolton JL. Alkylation of 2'-deoxynucleosides and DNA by the Premarin metabolite 4-hydroxyequilenin semiquinone radical. Chem Res Toxicol. 1998; 11:94–101. [PubMed: 9511900]
69. Embrechts J, Lemiere F, Van Dongen W, Esmans EL. Equilenin-2'-deoxynucleoside adducts: analysis with nano-liquid chromatography coupled to nano-electrospray tandem mass spectrometry. J Mass Spectrom. 2001; 36:317–328. [PubMed: 11312524]
70. Zhang F, Swanson SM, van Breemen RB, Liu X, Yang Y, Gu C, Bolton JL. Equine estrogen metabolite 4-hydroxyequilenin induces DNA damage in the rat mammary tissues: formation of single-strand breaks, apurinic sites, stable adducts, and oxidized bases. Chem Res Toxicol. 2001; 14:1654–1659. [PubMed: 11743748]
71. Embrechts J, Lemiere F, Van Dongen W, Esmans EL, Buytaert P, Van Marck E, Kockx M, Makar A. Detection of estrogen DNA-adducts in human breast tumor tissue and healthy tissue by combined nano LC-nano ES tandem mass spectrometry. J Am Soc Mass Spectrom. 2003; 14:482–491. [PubMed: 12745217]
72. Zhang N, Ding S, Kolbanovskiy A, Shastry A, Kuzmin VA, Bolton JL, Patel DJ, Broyde S, Geacintov NE. NMR and Computational Studies of Stereoisomeric Equine Estrogen-Derived DNA Cytidine Adducts in Oligonucleotide Duplexes: Opposite Orientations of Diastereomeric Forms. Biochemistry. 2009
73. Suzuki N, Yasui M, Santosh Laxmi YR, Ohmori H, Hanaoka F, Shibutani S. Translesion synthesis past equine estrogen-derived 2'-deoxycytidine DNA adducts by human DNA polymerases eta and kappa. Biochemistry. 2004; 43:11312–11320. [PubMed: 15366941]
74. Chen, D. Chemistry. New York University; 2007. Nucleotide Excision Repair and Translesion Synthesis of DNA Adducts Derived From the Equine Estrogen Metabolite 4-hydroxyequilenin.
75. Cadet J, Douki T, Ravanat J-L. Oxidatively Generated Damage to the Guanine Moiety of DNA: Mechanistic Aspects and Formation in Cells. Accounts of Chemical Research. 41:1075–1083. [PubMed: 18666785]
76. Adam W, Arnold MA, Grune M, Nau WM, Pischel U, Saha-Moller CR. Spiroiminodihydantoin is a major product in the photooxidation of 2'-deoxyguanosine by the triplet states and oxyl radicals generated from hydroxyacetophenone photolysis and dioxetane thermolysis. Org Lett. 2002; 4:537–540. [PubMed: 11843585]
77. Luo W, Muller JG, Rachlin EM, Burrows CJ. Characterization of spiroiminodihydantoin as a product of one-electron oxidation of 8-Oxo-7,8-dihydroguanosine. Org Lett. 2000; 2:613–616. [PubMed: 10814391]
78. Niles JC, Wishnok JS, Tannenbaum SR. Spiroiminodihydantoin is the major product of the 8-oxo-7,8-dihydroguanosine reaction with peroxynitrite in the presence of thiols and guanosine photooxidation by methylene blue. Org Lett. 2001; 3:963–966. [PubMed: 11277770]

79. Misiaszek R, Crean C, Geacintov NE, Shafirovich V. Combination of nitrogen dioxide radicals with 8-oxo-7,8-dihydroguanine and guanine radicals in DNA: oxidation and nitration end-products. J Am Chem Soc. 2005; 127:2191–2200. [PubMed: 15713097]
80. Jia L, Shafirovich V, Shapiro R, Geacintov NE, Broyde S. Spiroiminodihydantoin lesions derived from guanine oxidation: structures, energetics, and functional implications. Biochemistry. 2005; 44:6043–6051. [PubMed: 15835893]
81. Chinyengetere F, Jamieson ER. Impact of the oxidized guanine lesion spiroiminodihydantoin on the conformation and thermodynamic stability of a 15-mer DNA duplex. Biochemistry. 2008; 47:2584–2591. [PubMed: 18281959]
82. Kornyushyna O, Berges AM, Muller JG, Burrows CJ. In vitro nucleotide misinsertion opposite the oxidized guanosine lesions spiroiminodihydantoin and guanidinohydantoin and DNA synthesis past the lesions using Escherichia coli DNA polymerase I (Klenow fragment). Biochemistry. 2002; 41:15304–15314. [PubMed: 12484769]
83. Kornyushyna O, aB CJ. Effect of the oxidized guanosine lesions spiroiminodihydantoin and guanidinohydantoin on proofreading by escherichia coli DNA Polymerase I (Klenow Fragment) in different sequence contexts. Biochemistry. 2003; 42:13008–13018. [PubMed: 14596616]
84. Henderson PT, Delaney JC, Gu F, Tannenbaum SR, Essigmann JM. Oxidation of 7,8-dihydro-8-oxoguanine affords lesions that are potent sources of replication errors in vivo. Biochemistry. 2002; 41:914–921. [PubMed: 11790114]
85. Henderson PT, Delaney JC, Muller JG, Neeley WL, Tannenbaum SR, Burrows CJ, Essigmann JM. The hydantoin lesions formed from oxidation of 7,8-dihydro-8-oxoguanine are potent sources of replication errors in vivo. Biochemistry. 2003; 42:9257–9262. [PubMed: 12899611]
86. Neeley WL, Delaney S, Alekseyev YO, Jarosz DF, Delaney JC, Walker GC, Essigmann JM. DNA polymerase V allows bypass of toxic guanine oxidation products in vivo. Journal of Biological Chemistry. 2007; 282:12741–12748. [PubMed: 17322566]
87. Krishnamurthy N, Zhao XB, Burrows CJ, David SS. Superior removal of hydantoin lesions relative to other oxidized bases by the human DNA glycosylase hNEIL1. Biochemistry. 2008; 47:7137–7146. [PubMed: 18543945]
88. Hailer MK, Slade PG, Martin BD, Sugden KD. Nei deficient Escherichia coli are sensitive to chromate and accumulate the oxidized guanine lesion spiroiminodihydantoin. Chemical research in toxicology. 2005; 18:1378–1383. [PubMed: 16167829]
89. Goerigk L, Grimme S. Calculation of electronic circular dichroism spectra with time-dependent double-hybrid density functional theory. J Phys Chem A. 2009; 113:767–776. [PubMed: 19102628]
90. Tam MC, Russ NJ, Crawford TD. Coupled cluster calculations of optical rotatory dispersion of (S)-methyloxirane. Journal of Chemical Physics. 2004; 121:3550–3557. [PubMed: 15303920]
91. Polavarapu PL, Petrovic A, Wang F. Intrinsic rotation and molecular structure. Chirality. 2003; 15(Suppl):S143–S149. [PubMed: 12884385]
92. McCann DM, Stephens PJ. Determination of absolute configuration using density functional theory calculations of optical rotation and electronic circular dichroism: Chiral alkenes. Journal of Organic Chemistry. 2006; 71:6074–6098. [PubMed: 16872191]
93. Mori T, Inoue Y, Grimme S. Time dependent density functional theory calculations for electronic circular dichroism spectra and optical rotations of conformationally flexible chiral donor-acceptor dyad. Journal of Organic Chemistry. 2006; 71:9797–9806. [PubMed: 17168599]
94. Polavarapu PL, Zhao CX. Ab initio predictions of anomalous optical rotatory dispersion. Journal of the American Chemical Society. 1999; 121:246–247.
95. Giorgio E, Roje M, Tanaka K, Hamersak Z, Sunjic V, Nakanishi K, Rosini C, Berova N. Determination of the absolute configuration of flexible molecules by ab initio ORD calculations: A case study with cytoxazones and isocytoxazones. Journal of Organic Chemistry. 2005; 70:6557–6563. [PubMed: 16095271]
96. Crassous J, Jiang ZJ, Schurig V, Polavarapu PL. Preparation of (+)-chlorofluoroiodomethane, determination of its enantiomeric excess and of its absolute configuration. Tetrahedron-Asymmetry. 2004; 15:1995–2001.

97. Rinderspacher BC, Schreiner PR. Structure-property relationships of prototypical chiral compounds: Case studies. Journal of Physical Chemistry A. 2004; 108:2867–2870.

98. Norman P, Ruud K, Helgaker T. Density-functional theory calculations of optical rotatory dispersion in the nonresonant and resonant frequency regions. Journal of Chemical Physics. 2004; 120:5027–5035. [PubMed: 15267368]

99. Diedrich C, Grimme S. Systematic investigation of modern quantum chemical methods to predict electronic circular dichroism spectra. Journal of Physical Chemistry A. 2003; 107:2524–2539.

100. Pecul M, Ruud K, Helgaker T. Density functional theory calculation of electronic circular dichroism using London orbitals. Chemical Physics Letters. 2004; 388:110–119.

101. Iizuka E, Yang JT. Optical Rotatory Dispersion of L-Amino Acids in Acid Solution. Biochemistry. 1964; 3:1519–1524. [PubMed: 14231911]

102. Frisch, MJ.; Trucks, GW.; Schlegel, HB.; Scuseria, GE.; Robb, MA.; Cheeseman, JR.; Montgomery, JJA.; Vreven, T.; Kudin, KN.; Burant, JC.; Millam, JM.; Iyengar, SS.; Tomasi, J.; Barone, V.; Mennucci, B.; Cossi, M.; Scalmani, G.; Rega, N.; Petersson, GA.; Nakatsuji, H.; Hada, M.; Ehara, M.; Toyota, K.; Fukuda, R.; Hasegawa, J.; Ishida, M.; Nakajima, T.; Honda, Y.; Kitao, O.; Nakai, H.; Klene, M.; Li, X.; Knox, JE.; Hratchian, HP.; Cross, JB.; Bakken, V.; Adamo, C.; Jaramillo, J.; Gomperts, R.; Stratmann, RE.; Yazyev, O.; Austin, AJ.; Cammi, R.; Pomelli, C.; Ochterski, JW.; Ayala, PY.; Morokuma, K.; Voth, GA.; Salvador, P.; Dannenberg, JJ.; Zakrzewski, VG.; Dapprich, S.; Daniels, AD.; Strain, MC.; Farkas, O.; Malick, DK.; Rabuck, AD.; Raghavachari, K.; Foresman, JB.; Ortiz, JV.; Cui, Q.; Baboul, AG.; Clifford, S.; Cioslowski, J.; Stefanov, BB.; Liu, G.; Liashenko, A.; Piskorz, P.; Komaromi, I.; Martin, RL.; Fox, DJ.; Keith, T.; Al-Laham, MA.; Peng, CY.; Nanayakkara, A.; Challacombe, M.; Gill, PMW.; Johnson, B.; Chen, W.; Wong, MW.; Gonzalez, C.; Pople, JA. Gaussian. Wallingford CT: Gaussian, Inc.; 2004.

103. Karwowski B, Dupeyrat F, Bardet M, Ravanat JL, Krajewski P, Cadet J. Nuclear magnetic resonance studies of the 4R and 4S diastereomers of spiroiminodihydantoin 2'-deoxyribonucleosides: absolute configuration and conformational features. Chemical research in toxicology. 2006; 19:1357–1365. [PubMed: 17040105]

104. Mori T, Inoue Y, Grimme S. Quantum chemical study on the circular dichroism spectra and specific rotation of donor-acceptor cyclophanes. Journal of Physical Chemistry A. 2007; 111:7995–8006.

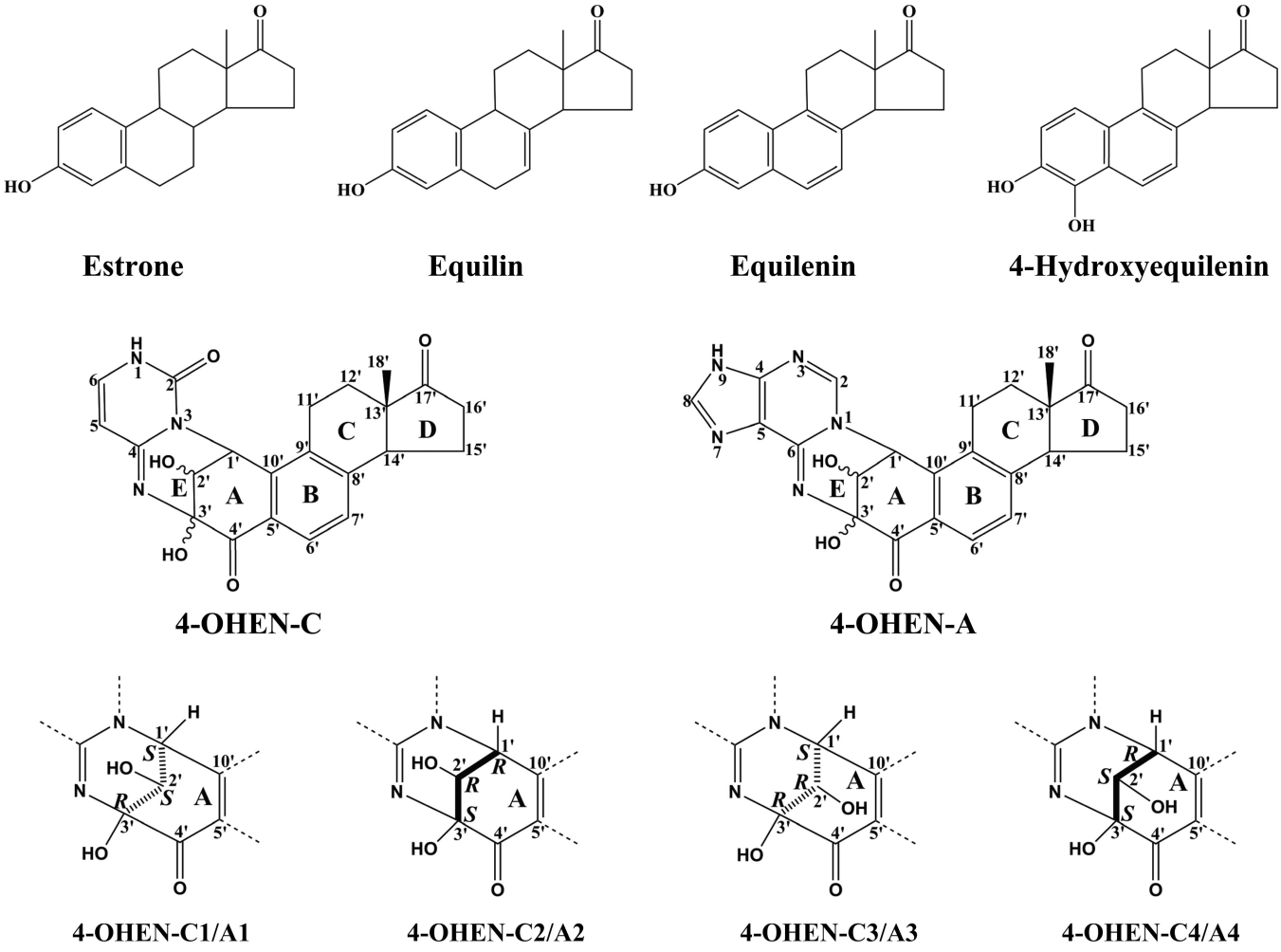

Figure 1.

Comparisons of chemical structures of estrone and equine estrogens, the metabolite 4-hydroxyequilenin, and the stereochemical properties of 4-OHEN-C and -A adducts.

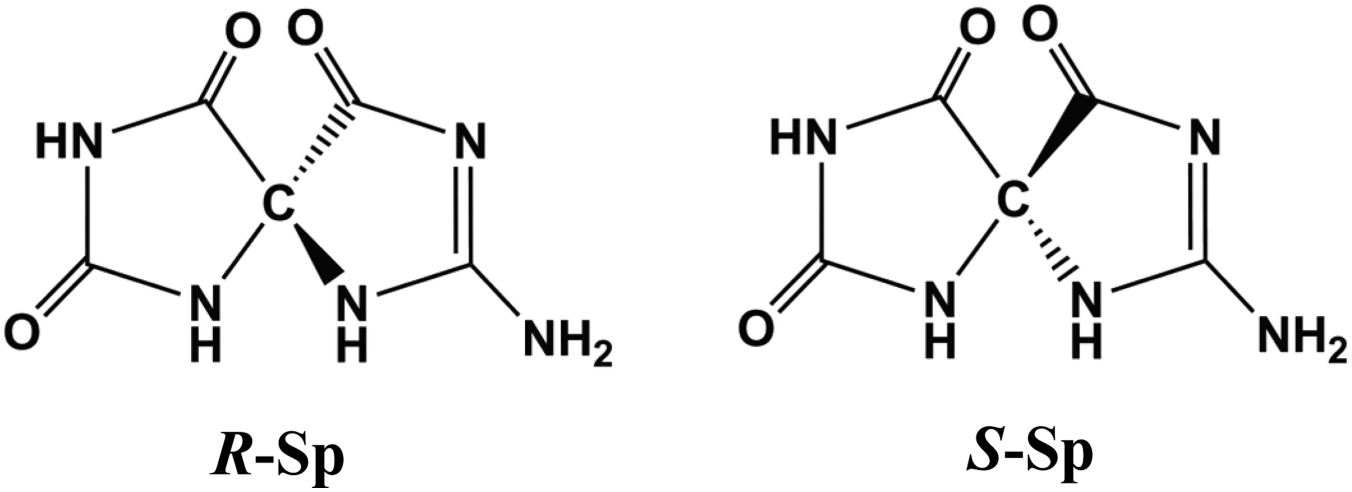

Figure 2.
Structures of spiroiminodihydantoins.

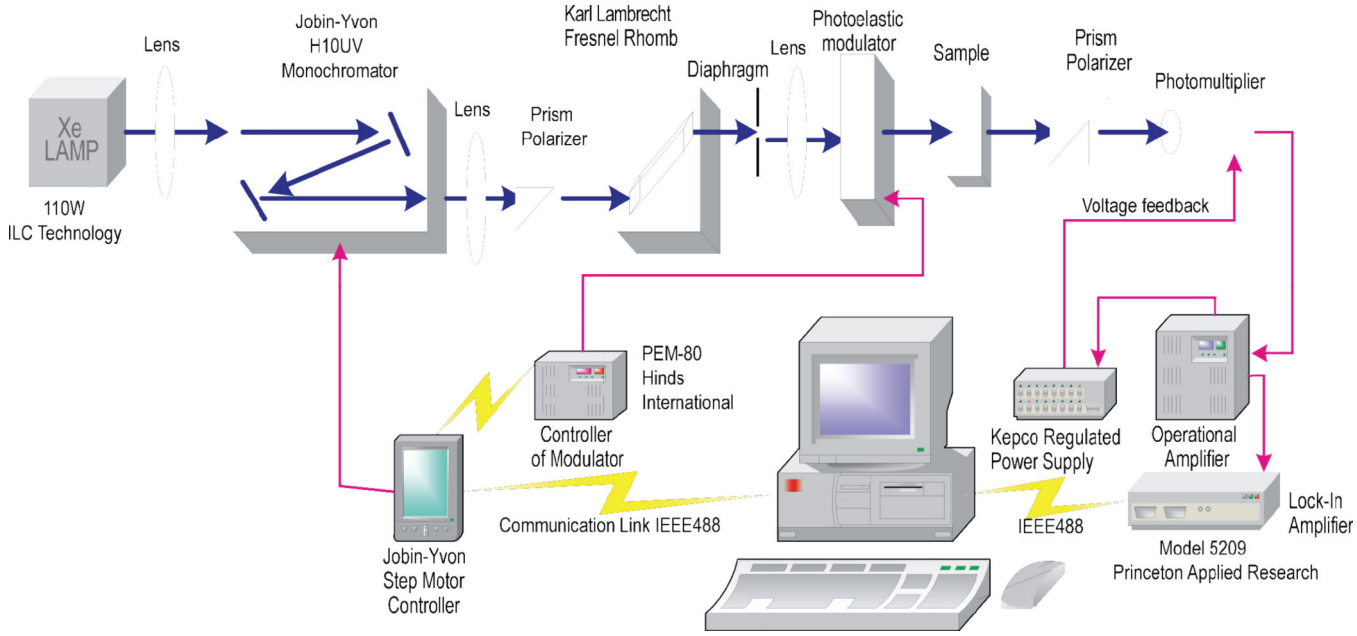

Figure 3.
Block diagram of ORD spectrometer.

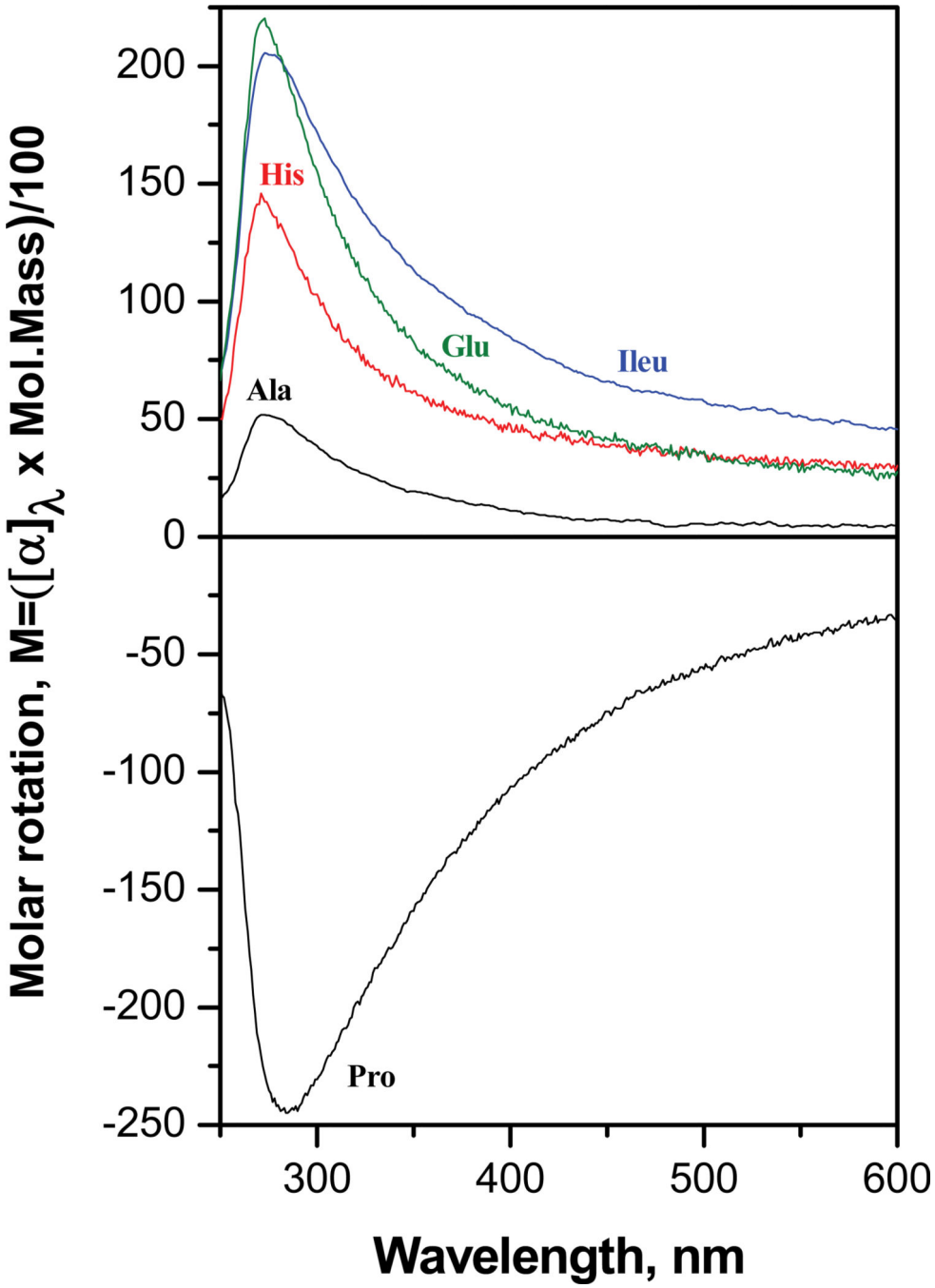

Figure 4.

ORD of amino acids measured using the apparatus depicted in Figure 3. Concentrations: 1g/100mL in 0.1N HCl. The results are presented in terms of molar rotation units to facilitate comparison with the previous work of Iizuka,E. and Yang, J.T., *Biochemistry*, 3, 1519 (1964).

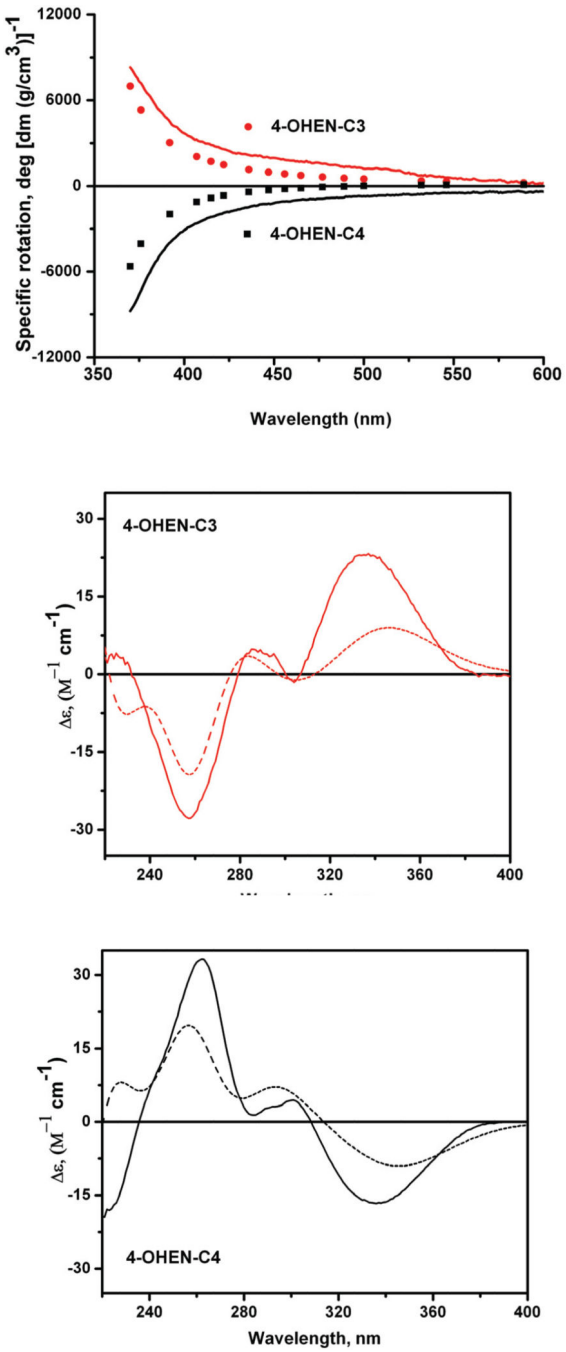

Figure 5.

Top panel: Comparisons of computed 4-OHEN-C3 and -C4 adduct ORD spectra (circles) and experimentally measured ORD spectra (solid lines) of C^3 and C^4 adducts (see the text). Middle and bottom panels: Computed 4-OHEN-C3 and -C4 adduct ECD spectra (dashed lines), and comparisons with experimentally measured ECD spectra (solid lines) of C^3 and C^4 adducts (see the text).

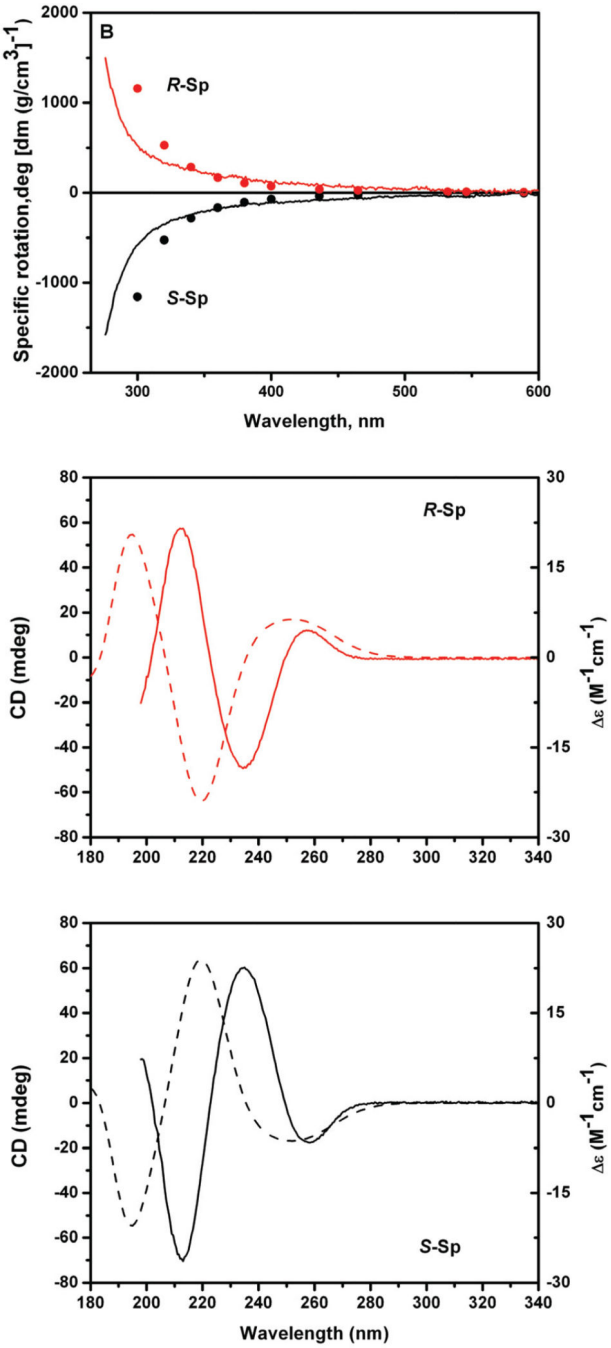

Figure 6.

Top panel: Comparisons of computed *S*- and *R*-Sp ORD spectra (circles), and experimentally measured ORD spectra (solid lines). Middle and bottom panels: Computed *R*- and *S*-Sp ECD spectra (dashed lines), and comparisons with experimentally measured ECD spectra (solid lines). The experimental CD spectra are expressed in mdeg/per absorbance unit at 230 nm (1.0 cm optical pathlength).